

the smaller mangrove sites, including KII Ecopark, Aklan (80%), Balangkayan, Samar (80%) and Triboa Mangrove Park (87%). The KII Ecopark is 45 ha while Triboa is only around two hectares. The accuracy within the said sites are seen to be affected by the spatial resolution of the input Sentinel-2 image which is in 10 m resolution, while the drone data is at few centimeters. Some of the validation points are located within Sentinel-2 mixed pixels, which can only be separated in the higher resolution validation data. Lower accuracy in KII Ecopark could also be influenced by the tide level during the satellite acquisition as a large area of the forest is exposed during low tide.

Table 5.

Accuracy of MVI in discriminating mangroves from non-mangrove pixels, computed using mangrove validation pixels from drone orthophotos and field-acquired tree locations. The highest accuracy was derived from Palawan sites (Coron, Busuanga and Puerto Princesa) while the lowest values were derived from Katunggan-It Ibajay, Aklan and Eastern Samar, two of the smallest study sites.

| Study Site | Coverage of Validation Data | Accuracy (%) |
|---------------------------------|--------------------------------|--------------|
| Coron-Busuanga | Calauit Island | 94 |
| | Bintuan (Coron) | 96 |
| | Sagrada and Bogtong (Busuanga) | 100 |
| Puerto Princesa, Palawan | Bacungan | 98 |
| | Banate Bay, Iloilo | 90 |
| | Bancal Bay, Iloilo | 98 |
| Panay Island | Katunggan-It Ibajay, Aklan | 80 |
| | Bakhawan Ecopark, Aklan | 96 |
| Zambales | Triboa Mangrove Park, Subic | 87 |
| | Baloganon, Masinloc | 90 |
| Eastern Samar | Balangkayan | 80 |
| Fukido, Ishigaki | Fukido Mangrove Park | 92 |
| <i>Overall Average Accuracy</i> | | 92 |

Meanwhile, few mixed pixels consisting of healthy and damaged/dead mangroves in the Balangkayan site could have lessen the MVI accuracy. Pure ‘damaged to dead mangrove pixels’ have lower reflectance in the NIR region and higher in the green, so the resulting MVI is lower. The decrease in NIR reflectance is caused by the absence of healthy leaf tissues, while the increase in green is driven by the inability of stressed vegetation to absorb visible light (Kovacs et al., 2001). Samples of the pure dead mangroves pixels in Balangkayan have MVI values ranging from 0.9 to 1.5, while mixed healthy and dead mangroves pixels have an MVI ranging from 1.9 to 4.6, depending on the ratio of the dead and alive mangroves per Sentinel-2 pixel. All pure mangrove pixels have an MVI values higher than 4.5.

3.5 Application to Landsat Data

Prior to MVI comparison between Sentinel-2 and Landsat data, the agreement between the input bands were determined first by obtaining sample reflectance values in the green, NIR and SWIR1 regions. Three land cover classes (Figure 11) were included in the analysis: mangroves, non-mangrove vegetation such as forest and grass, and non-vegetation which includes built-up and bare soil.

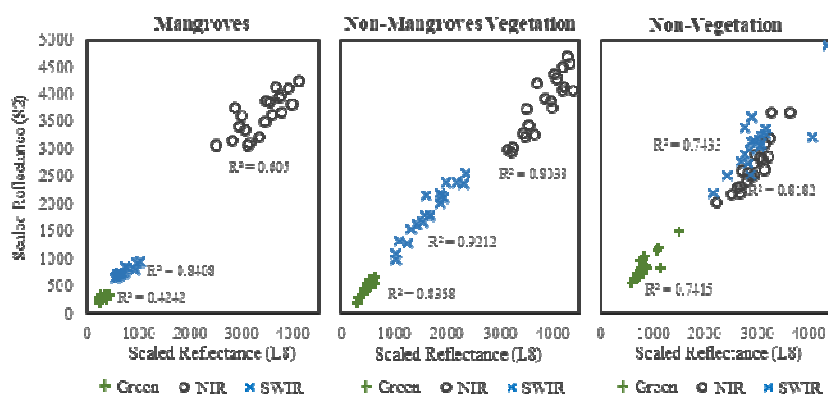


Fig. 11. Spectral fit of the green, NIR and SWIR1 bands between the mangroves and non-mangroves classes derived from atmospherically corrected Landsat-8 and Sentinel-2 images of Calauit Island acquired February 15, 2016 and February 12, 2016

Results show that the green, NIR and SWIR1 bands of the input Landsat and Sentinel bands have overall good spectral fit with R^2 values between 0.42 and 0.92. The highest linear fit was obtained from the non-mangrove vegetation samples as observed in all three bands ($R^2 = 0.80$ to 0.92). In mangroves, moderate agreement was obtained in the green ($R^2=0.42$) and NIR region ($R^2=0.60$), but high in the SWIR1 region ($R^2=80$). This implies that we can expect some degree of differences in the output Landsat-based and Sentinel-based MVI images. Low spectral fit in mangroves’ NIR can be attributed to the narrower spectrum of the Landsat NIR which was intended to avoid heavy water contamination (Li et al., 2017). The spectral bandwidth of Landsat-8 and Sentinel-2 NIR is

0.028 and 0.033 μm , respectively. Other variations between the two sensors can be attributed to factors such as heterogeneous terrain, mixed pixels (Runge and Grosse, 2019) and the algorithms used in converting TOA to surface reflectance (Claverie et al., 2018). Between the three classes shown in Figure 11, the green and SWIR1 values are both lowest in mangroves, as previously observed in Coron-Busuanga dataset. Low green values will help discriminate mangrove greenness while low SWIR1 values separate vegetation from non-vegetation, and moisture-rich vegetation from dry vegetation. The NIR values are more scattered within the mangrove class as the selected sample plots have different cover density.

The MVI formula was applied to Landsat data using the equivalent green, NIR and SWIR1 bands (Figure 12). The Landsat MVI and Sentinel-2 MVI generated comparable mangrove maps, with similar locations of mangrove forests being highlighted as seen in Figure 12-B. The Landsat threshold was found to be close with Sentinel-2, with a minimum MVI value of 4.5 and a mean value of 8.6 (Figure 12-A). Most sample plots, however, have higher Landsat MVI than Sentinel which can be attributed to the observed differences in Figure 11. Meanwhile, the mean Sentinel-2 MVI from Calauit plots is 7.4 which is very close to the mean MVI obtained from the main Coron-Busuanga Island (7.5). Similar to Sentinel, the 4.5 minimum threshold for Landsat can already discriminate the mangrove areas from bare soil, built-up, terrestrial forest and other terrestrial vegetation cover. However, the obtained maximum MVI threshold of non-mangrove vegetation pixels reach 4.5, so it is suggested to use 4.6 as the safe minimum threshold for Landsat-based MVI mangrove mapping in the selected site.

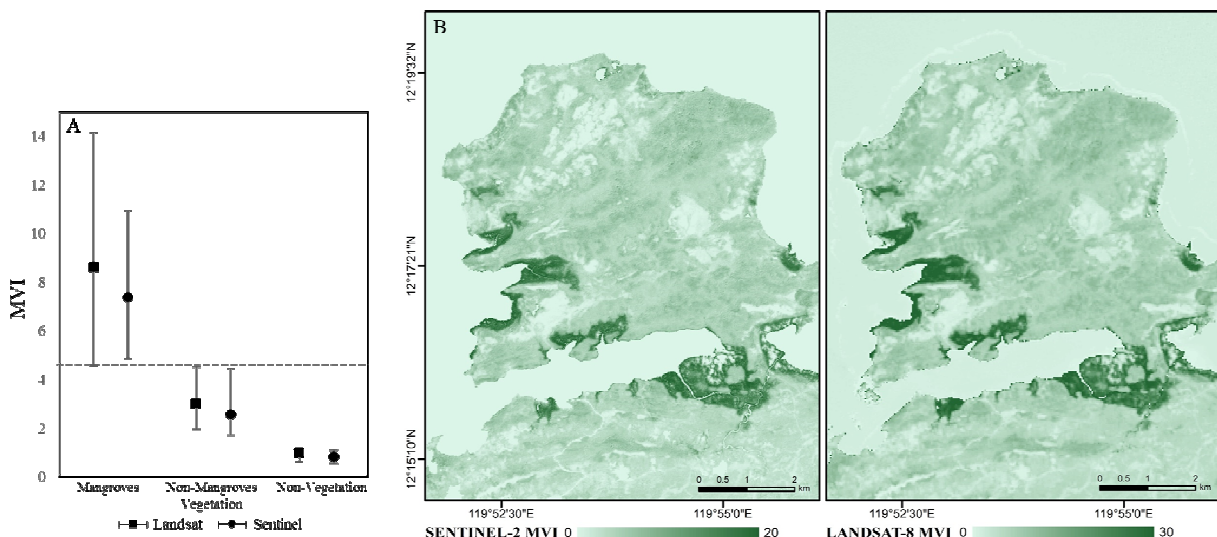


Fig. 12. **A.** Mean, maximum and minimum Landsat and Sentinel MVI values of mangroves, non-mangroves vegetation and non-vegetation land cover in Calauit Island, Busuanga (graph, left). The minimum threshold for mangrove MVI was observed to be 4.5, but an optimal threshold of 4.6 is suggested as the maximum threshold of non-mangrove vegetation is also 4.5 (Landsat). Overall, the Landsat MVI has wider threshold range than Sentinel-derived MVI. **B.** MVI images generated for Sentinel (map, left) and Landsat (map, right) using the equivalent green, NIR and SWIR bands. The locations of the mangrove areas are found to be similar in both data despite the difference in spatial resolution.

3.6 Comparison with General Vegetation Indices

NDVI, LAI and FVC are good indicators of vegetation health. FVC corresponds to the gap fraction for nadir direction, used to separate vegetation and soil in energy balance processes including temperature and evapotranspiration. It is one of the basic ecological characteristics which can provide quantitative information of the vegetation coverage status on the ground (Li et al, 2015). LAI is defined as half the developed area of photosynthetically active elements of the vegetation per unit horizontal ground area. Variations of LAI in mangrove ecosystems reflects the different environmental forces acting upon each location (Araujo et al, 1997). There are limitations in using of NDVI, LAI and FVC for vegetation discrimination because similar index values can be obtained for all healthy vegetation, regardless of forest type and mangroves species composition (Alsaideh et al., 2013; Kongwongjan, et al, 2012). The NDVI, LAI and FVC images are shown with MVI in Figure 13. Unlike other vegetation indices, MVI is a mangrove-specific index which can distinguish mangrove from non-mangrove vegetation. High NDVI means healthier and greener vegetation, and similarly, high MVI can reflect healthier mangrove leaf structures (higher NIR reflectance) and more leaf green pigments (higher green reflectance). Higher MVI can also signify efficient radiation absorption by the water in healthy leaves which can be detected in the SWIR region. Candidate stressed mangrove trees from the study sites gave lower MVI values, while totally damaged and dead trees generated an MVI value outside the mangrove threshold (MVI < 4.5).

The study further analyzed if the MVI range (4.5 and higher) is specifically dependent on mangrove health, so as to conclude if (a) increasing MVI level always means increasing mangrove vigour or (b) increasing MVI means higher probability of a land cover pixel being a mangrove, as affected by canopy greenness and moisture. To facilitate this analysis, candidate mangrove pixels were obtained from two forest types: riverine and fringe mangrove forests. Fringe mangrove forests are directly exposed to the tides and sea waves, while riverine mangroves are flooded by most high tides and dry up at most low tides. Although fringe mangroves are more inundated, the condition within riverine forest are more optimal for healthier growth because of freshwater runoff, nutrient

influx, moderate salinity level (Ewel et al., 1998) and low tidal energy (Cunha-Lignon et al., 2011). Riverine mangroves are reported to be among the most productive trees (Ewel et al., 1998) which are significantly denser than the fringe type (Nugroho et al., 2019).

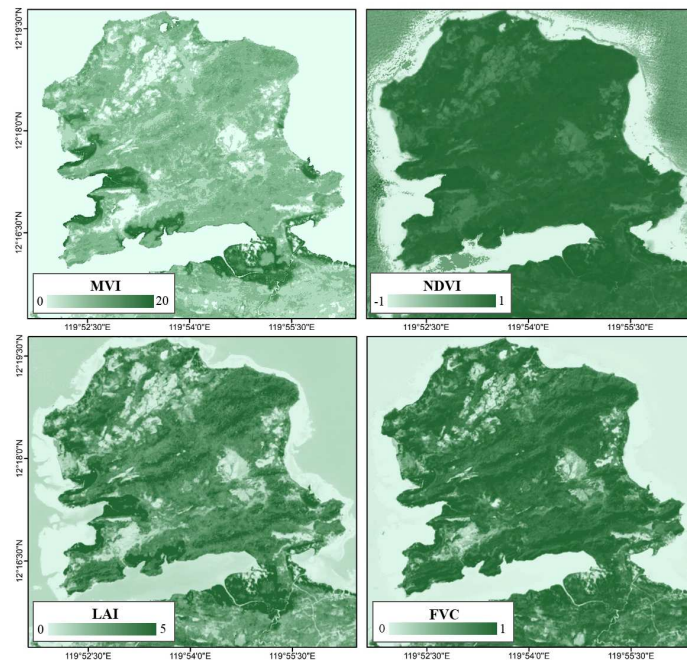


Fig. 13. Mangrove Vegetation Index (MVI) and the generated vegetation indices from Sentinel-2: NDVI, LAI and FVC. High index values were observed within vegetation cover such as mangroves and terrestrial forests, except for MVI which generated high index value solely for mangroves and lower values for non-mangrove vegetation.

The result shows that mean LAI, FVC, and NDVI are all higher in the riverine forest (Table 6) in agreement with previous studies. The trend for mean MVI is opposite, which is higher in the fringe forests (MVI=8.9) than in the riverine (MVI=6.7). This implies that the difference in inundation and background moisture properties between the two forest types could have affected the mangrove MVI values more than leaf health, as reflected by lower mean LAI, FVC and NDVI in the fringe mangroves.

Table 6.

Mean MVI, LAI, FV and NDVI values obtained from riverine and fringe mangrove forests, and correlation ($\alpha=0.05$) of the three general vegetation indices with the respective MVI generated for each forest type. Higher MVI was obtained from the fringe mangrove type.

| Variable | Riverine Mangrove Forest | | | | Fringe Mangrove Forest | | | |
|--------------------------|--------------------------|-----|------|------|------------------------|-----|-----|------|
| | MVI | LAI | FVC | NDVI | MVI | LAI | FVC | NDVI |
| Mean index value | 6.7 | 4.1 | 0.79 | 0.73 | 8.9 | 3.7 | 0.7 | 0.69 |
| Correlation (r) with MVI | - | 0.4 | 0.5 | 0.04 | - | 0.2 | 0.3 | 0.3 |

Only riverine mangroves MVI and FVC have moderate positive correlation ($r=0.5$), while correlation values between MVI and LAI ($r=0.4$) and NDVI ($r=0.04$) are lower. The positive correlation of MVI with FVC and LAI regardless of mangrove forest type implies that all of these indices can reflect the presence and size of a plant photosynthetic area where the leaf greenness and moisture information are obtained. The correlation of NDVI with MVI is higher in the fringe forest ($r=0.3$) which could be attributed to the full structural development of seafront mangroves species due to frequent flooding (Cunha-Lignon et al., 2011).

MVI is positively correlated with health indicators such as LAI, FVC and NDVI but was also found to be sensitive to biophysical variations within different mangrove forest types. It was observed that higher MVI values reflects higher probability of an image pixel to be a ‘mangrove’ rather than solely indicating better vegetation health. Greener vegetation, more leaf water content, and added effect of background soil moisture in the SWIR region as affected by its coastal habitat (Zhang and Tian, 2013) will result to higher MVI. Nevertheless, mangroves captured with less background moisture during low tide will still generate an MVI within the mangrove threshold due to their ability to store enough moisture in the leaves (Camilleri and Ribi, 1983; Nguyen et al., 2017; Reef and Lovelock, 2014). In riverine and other landward mangrove forests, the available less-saline water sources become the main source of water in the xylem as a mechanism to avoid cavitation and regulate water loss (Reef and Lovelock, 2014).

3.7 Comparison with Sentinel-2 derived Chlorophyll-a and Canopy water

The chlorophyll-a (C_a) and canopy water (C_w) layers were derived from Sentinel-2 through the SNAP biophysical toolbox SNAP toolbox using tested, generic algorithms based on specific radiative transfer models. C_a is considered as the central photosynthesis

pigment as it is a constituent of the photosynthetic reaction center. C_w content is defined as the mass of water per unit ground area, which also relies on the water absorption features centered at 970 nm, 1,200 nm, 1,450 nm and 1,950 nm (Raven et al. 1992). Sentinel's C_w and C_a determine greenness and canopy moisture content which are similar to the biophysical variables considered in generating MVI. For this reason, the study identified the correlation of MVI's greenness equation (NIR-green) with C_a , MVI's moisture equation (SWIR1-green) with C_w , and the output MVI with C_a and C_w . The Sentinel-2 derived C_a and C_w are already quality-controlled data generated using validated models (Fourty and Baret 1997; Jacquemoud and Baret 1990; Newnham and Burt 2001, Weiss, 2018). The result shows high correlation ($\alpha=0.05$) of MVI with C_w ($r=0.84$) and C_a ($r=0.63$) which suggest that the MVI can efficiently measure leaf canopy greenness and moisture (Figure 14). The MVI greenness and moisture equations alone generated moderate to strong linear relationship with C_a ($r=0.73$) and C_w ($r=0.6$). As observed with MVI, C_w levels were reported to be affected also by soil moisture (Weiss, 2018) and this similarity may have sustained the positive correlation between the two data.

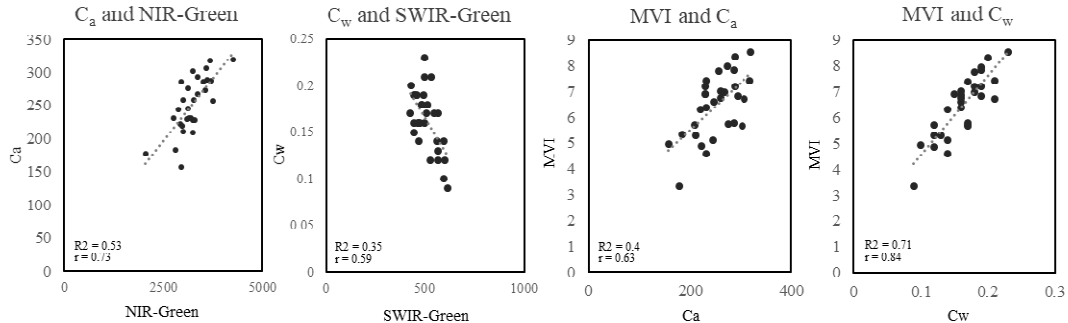


Fig. 14. Correlation between MVI's greenness equation (NIR-green) and C_a , moisture equation (SWIR1-green) and C_w , and resulting MVI values with C_a and C_w . The MVI has moderate positive linear relationship with C_a ($r=0.63$) and strong positive correlation with C_w ($r=0.84$). This explains that the MVI is a good indicator of canopy greenness and moisture and can be used an alternative to Sentinel-2 C_a and C_w products for mangrove biophysical analysis. Data for NIR, green and SWIR1 are scaled reflectance ($\times 10,000$).

3.8 IDL and Google Earth Engine-based MVI Mapping

The IDL platform for offline MVI processing was designed to process offline the available Sentinel-2 input data. The user will need to input the directory of the stacked pre-processed Sentinel-2 bands, the scene qualification data, the lower and upper threshold and the directory for the output folder. The output folder will contain the generated products including the MVI vegetation raster (vegetation masked), the MVI mangrove raster (threshold applied) and the Mangrove shapefile that can already be exported to mapping software for quality check and map layout. The processing time is fast, wherein MVI generation for the whole scene covering Coron-Busuanga only took 3 minutes. Processing of other subsites ranges from 1 to 18 minutes, depending on the size of terrestrial cover per Sentinel-2 scene. The IDL-based mapper eliminates the manual processes to facilitate faster product generation.

The Google Earth Engine MVI Mapper (Figure 15) was designed to have a user-friendly interface. The user can select the desire Sentinel-2 tiles, start and end date of data acquisition, and the target products. There are four products initially listed: the RGB image, the False Color Composite image, the masked vegetation raster and the aster and the mangrove raster. The earliest data that can be selected is March 28, 2017 which is the earliest available date for the Sentinel-2 Multi-Spectral Instrument Level-2A datasets in Google Earth Engine catalogue. Similar with the atmospheric correction algorithm applied in the study sites using SNAP, the said database from GEE is also processed with sen2cor. After running the script, the MVI Mapper will display all available images within the date range. With the aid of RGB and FCC, the user can easily navigate and select the best MVI raster layer with minimum cloud, cloud shadow and haze cover. All four products can be downloaded by clicking on the selected image filename.

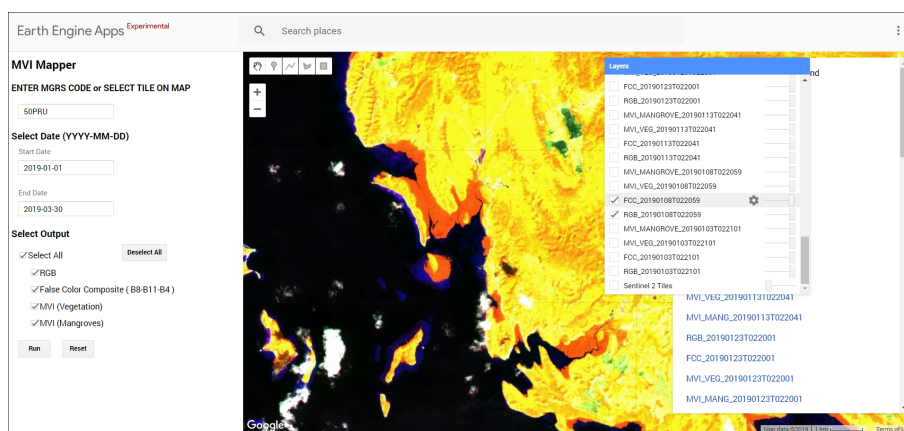


Fig. 15. Google Earth Engine-based Mangrove Mapper interface generated to process online the available Sentinel-2 input data. The four products include RGB, FCC, vegetation MVI raster and mangrove MVI raster. All available data will be displayed.

Both the IDL and GEE MVI Mapper will be available for public use. Continuous improvement and updates will be made by the researchers. For the latest version of GEE MVI Mapper, the user can already input the desired lower and upper MVI threshold for mangrove mapping to preview the MVI product before download.

3.9 MVI Application for Nationwide Mapping

Mangroves are distributed throughout the Philippines islands, covered by more than 100 Sentinel tiles. The latest estimate of mangroves in the Philippines is still for year 2016, with a total 220,984 ha (Bunting et al., 2018). The Google Earth Engine GUI was utilized in generating the updated mangrove maps of the country for year 2019. The boundary shapefile for each Military Grid Reference System (MGRS) code for each Sentinel tile was uploaded for faster selection of area. For each tile, the clearest MVI output was selected by displaying it in the GUI map. Based on the results, a combination of clean and contaminated MVIs are obtained within the said year.

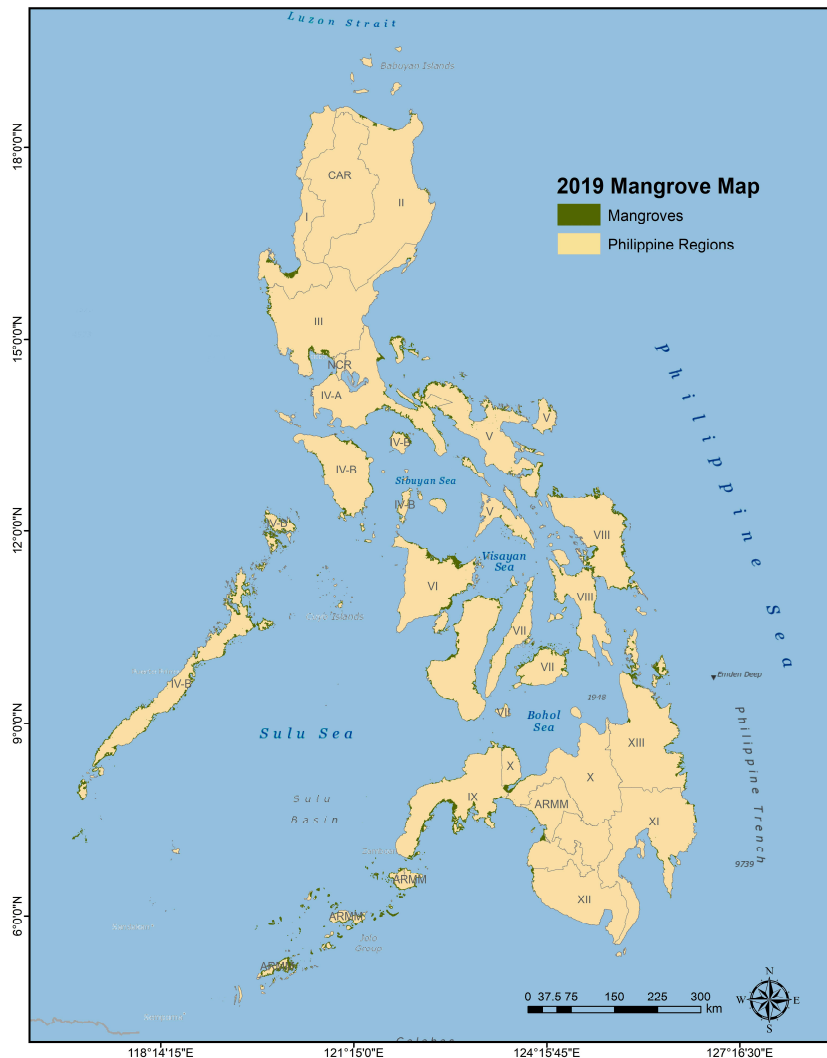


Fig. 16. MVI-based mangrove extent map of the Philippines generated from Sentinel-2 imagery using Google Earth Engine-based MVI Mapper. This map has a spatial resolution of 10m. The computed total mangrove extent is 227,808 ha for year 2019.

Users must navigate first the list of the displayed result (Figure 15, right panel) and identify the image date with no or less clouds, haze and cloud shadows. The thin haze over dense vegetation tend to generate similar values with MVI, although it is not perpetual among all haze cover. The clouds and cloud shadows can conceal the target mangrove areas and thus can affect the total area in case of mangrove mapping. Out of the 107 tiles covering the country, MVI output was downloaded for 87 tiles. Some mangroves areas are found within the overlap of two Sentinel tiles. Most of the clear images were acquired on the months of April (20 tiles), August and September (15 tiles). No MVI image acquired during the wet season was downloaded such as December, January and February due to the persistence of clouds and haze in the images. In areas with persistent clouds and shadows, additional data from other months were used to fill in the data gaps. In the absence of other clear images, some polygons from GMW were used for the remaining gaps. The output MVI layers were cleaned from noise pixels and was merged into a map showing the updated mangrove extent of the Philippines (Figure 16). A total of 227,808 ha of mangrove area was obtained (2019), close to the previous

estimates by GMW 2016 (220,984 ha), lower than Long and Giri (240,824 ha) and higher than the UP Phil-LIDAR Landsat-based estimate (208,020 ha).

3.10 Application to Other Mangrove Forests in Southeast Asia

The IDL-based MVI Mapper was utilized to test the application of MVI in mapping the mangroves from four other countries in Southeast Asia in addition to the study site in Ishigaki, Japan. These are Thailand, Vietnam, Indonesia and Cambodia. Mangrove forests in Thailand are located on muddy tidal flats at river mouths and along the coasts specifically on the Gulf of Thailand ([Pumijumnong, 2014](#)). The selected site for this study is the mangrove forest in Mueang Trat District in Trat, the easternmost province along the Thailand coast. The chosen Vietnam site is the Can Gio mangrove forest located in Ho Chi Minh City while mangrove forest in Kubu Raya Regency, West Kalimantan was chosen for MVI application in Indonesia. Can Gio is the largest restored mangrove forest in Vietnam ([Hung et al., 2018](#)) which was recognised as the first biosphere reserve in Vietnam by UNESCO in the year 2000. The terrain is flat and tide is semi-diurnal. The tile covering the mangroves forests in West Kalimantan include protected coastal and riverine mangroves such as those found in Muara Kubu and Batu Ampar. In Cambodia, mangroves can only be found in Southwestern part of the country covering four provinces: Koh Kong, Preah Sihanouk, Kompot and Kep ([Tieng et al, 2019](#)). Mangrove forest located in Prey Nob was selected which include the Ream National Park.

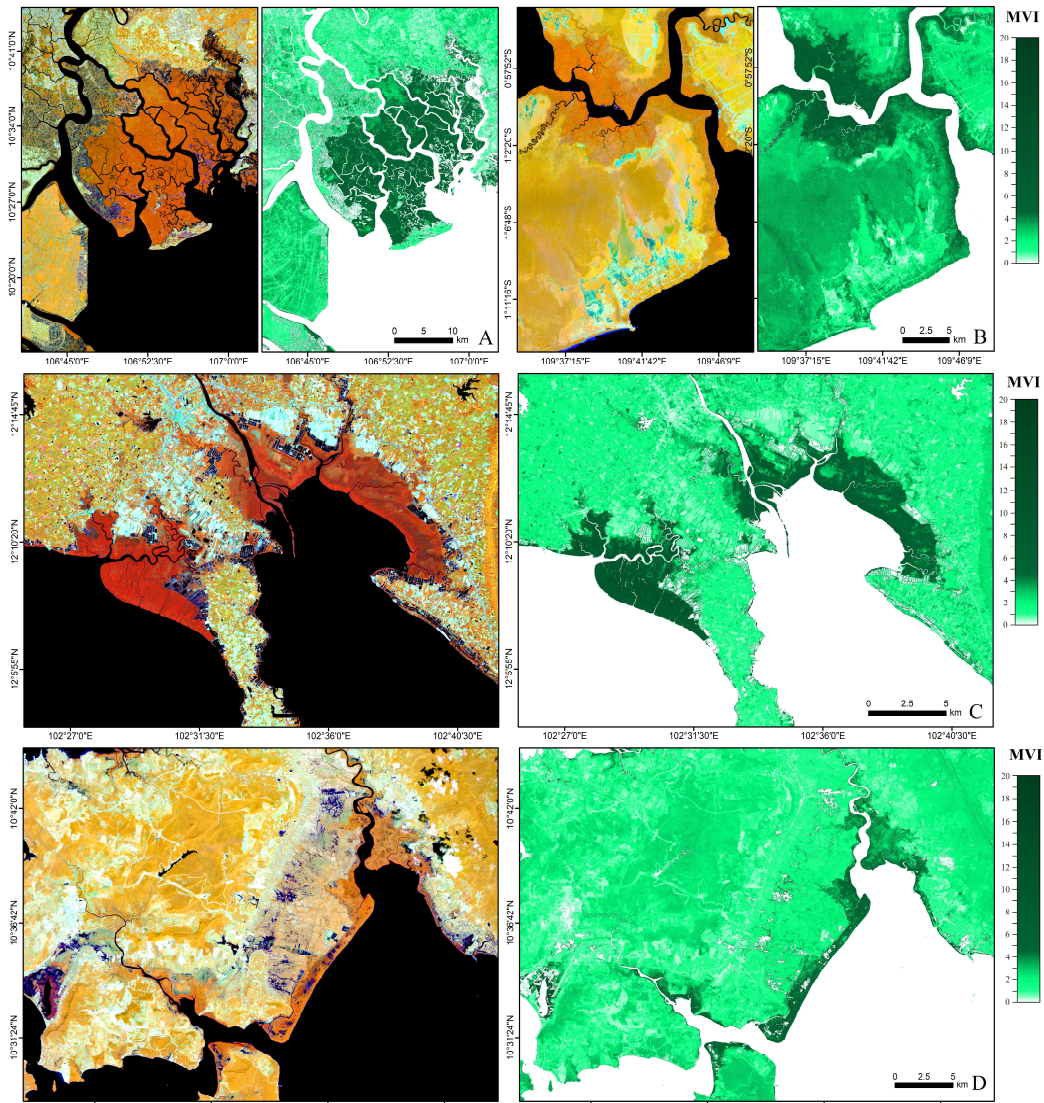


Fig. 17. False color composite visualization and MVI images of generated from Sentinel-2 covering (A) Can Gio Mangrove Forest, Ho Chi Minh City, Vietnam, (B) Muara Kubu and Batu Ampar, West Kalimantan, Indonesia, (C) Mueang Trat District, Trat, Thailand, and (D) Prey Nob, Cambodia. A different threshold was selected for each study site due to the unique coastal environment.

The selected optimal minimum threshold is 3.5 for the sites in Vietnam and Indonesia, and 3 for Cambodia and Thailand, both situated on the Gulf of Thailand. These thresholds are lower than the 4.5 threshold in the Philippine study sites, but similar and close to average lower threshold (3.5) used for the smaller and less dense mangrove forests in the nationwide mangrove map. Comparison of the Philippine mangrove dataset with the Thailand, Vietnam and Cambodia showed that the differences in the MVI threshold are more driven by the difference in the dividend or the greenness equation than moisture variation. Higher mean NIR reflectance values

were recorded from the Philippine site (0.35) as compared to Vietnam (0.31), Thailand (0.28), and Cambodia (0.23). High NIR reflectance is associated to high canopy density, thicker leaves and dense mangrove stands (Patterson, 1986; Zhang, 2014). In the Philippines, high mangrove density was previously observed from sample sites with FVC values ranging from 0.7 to 0.79 in fringe and riverine mangrove stands, respectively (Table 6). Meanwhile, the FVC of Vietnam, Thailand, and Cambodia is lower, with mean values of 0.67, 0.62, and 0.56, respectively. Sites with drier mangrove substrates will also result to lower MVI values due to the increase in SWIR1 reflectance, thus increasing the MVI denominator value. This was the factor observed in Indonesia, with mean NIR (0.36) and mean FVC (0.74) values close to that of the Philippines, but with higher moisture equation difference due to higher SWIR1 mean reflectance (0.1) compared to the later (0.07). To facilitate faster selection of threshold, the researchers added a threshold setting option in the GEE MVI Mapper to allow users to preview the MVI output per selected threshold as overlaid to the false color images.

Using IDL-based MVI Mapper, a total of 8,010 ha of mangroves was computed in Trat, Thailand, close to the previously estimated value of 8,190 ha for year 2017 using Landsat data (Pimple et al., 2018), and lower than GMW's estimate of 8,375 for year 2016 (Bunting et al., 2018). For Can Gio, Vietnam, the MVI-based mangrove area estimate is 35,353 ha, close to the estimated values of 35,000 ha in 2017 (HCMC, 2017), and lower than the estimated 38,164 ha in 2016 by GMW (Bunting et al., 2018) and in 2011 using SPOT 4 and 5 images: 40,074 ha (Pham et al., 2019). The estimate for the Cambodia site varies based on MVI for year 2019 (6,688 ha), GMW map for year 2016 (9,520 ha) and Landsat-based Random Forest (RF) classified map for years 2014-2015 (13,891) (Tieng et al., 2019). For Indonesia, the total area of the mangrove region shown in Figure 17 is 17,176 ha. Data cleaning was done due to the persistence of haze and cloud in the images, especially for the Indonesia site.

3.11 Application to Mangrove Forests outside Asia

The MVI maps of three additional sites namely Baía de São José, Amazon Coast in Brazil, Mabokweni in Tazania, and Prince Regent National Park in Western Australia were generated using the IDL software. Baía de São José is a bay in northeastern Brazil housing the Maranhão mangroves. The area is known to be macrotidal, with tidal amplitude between 4 m and 7.5 m (Souza-Filho, 2005). Meanwhile, mangrove forests in Mabokweni, Tazania occurred along the continental coast of Eastern Africa which houses greater diversity of mangrove species than those located in the west. The third mangrove site is Prince Regent National Park, a UNESCO Biosphere Reserve newly incorporated to the Kimberley National Park. The mangroves in the Kimberley coast occurs in tidal flats, tidal creeks, spits, high-tidal alluvial fans, or in rocky-shore ravines (Cresswell & Semeniuk, 2011).

The mangrove sites of Baía de São José, Mabokweni and Prince Regent National Park (Figure 18) were found to have an optimum minimum threshold of 3 for MVI mapping. This threshold is similar with that of Prey Nob, Cambodia and Trat, Thailand (Table 7). Compared with the Philippines, the mean MVI generated by said sites are lower, with MVI=4, 6.5 and 5.7, respectively. The lowest mean MVI (MVI=4) was computed from Baía de São José, the site with high tidal amplitude. Among the three, the lowest SWIR (0.07) was obtained from Prince Regent National Park which could be induced by the presence of freshwater seepages in the Kimberley Coast (Cresswell & Semeniuk, 2011). The FVC and NIR is also lower compared to that of the Philippines. The

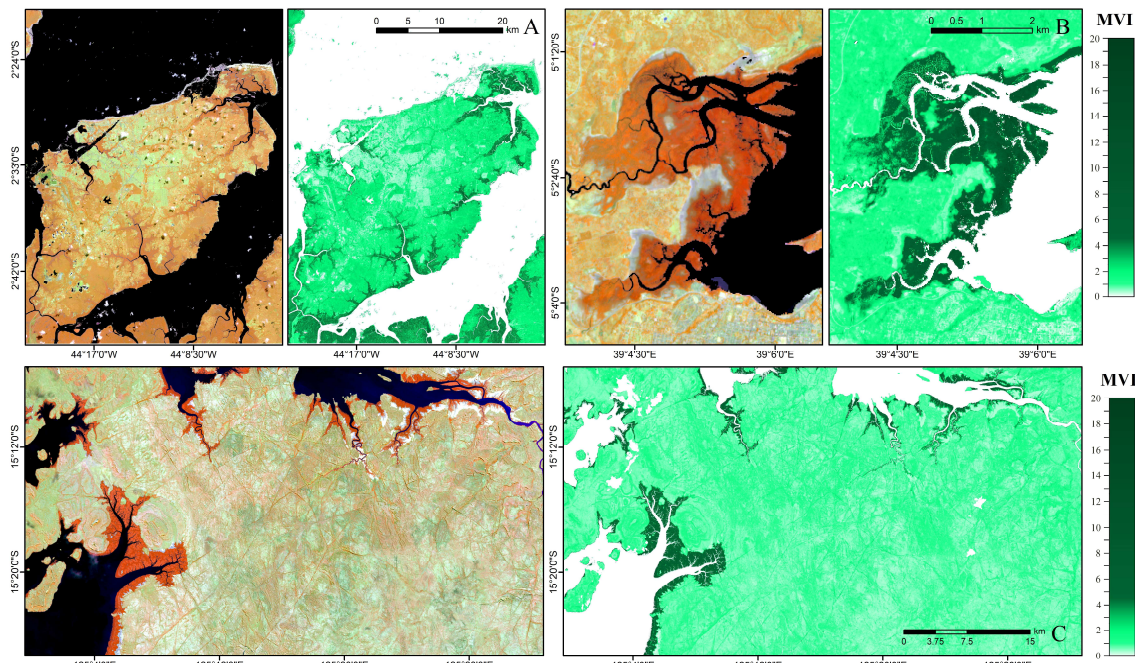


Figure 18. False color visualization and Sentinel-2 MVI images covering three mangrove sites outside Asia: (A) Baía de São José, Amazon Coast, Brazil, (B) Mabokweni, Tazania, and (C) Prince Regent National Park, Western Australia. Similar optimum lower MVI mangrove threshold were computed between the mangrove sites.

FVC of Baía de São José, Mabokweni, and Regent National Park are 0.64, 0.59, and 0.51, respectively, while Philippine sites' FVC is above 7. The total mangrove areas of the site coverage as shown in Figure 18 are 21,984 ha for Baía de São José, 824 ha for Mabokweni, and 13,926 ha for Regent National Park.

There is no clear pattern on the minimum MVI threshold on the basis of latitudinal differences (Table 7). The lower MVI threshold was found to have a very narrow range from 3 to 3.5, despite differences in mangrove typology and geographical coordinates among the sites. This observation highlights the potential of MVI for global-scale mangrove mapping using standard sets of thresholds. Mabokweni and Prince Regent National Park, both estuarine mangroves, utilized a threshold of 3. Mangrove thriving near estuaries and rivers are known to receive higher amount of nutrients but may also be limited by factors such as slow rate of belowground production (Lovelock et al, 2009). Meanwhile, delta mangroves in the Vietnam and Indonesia sites were best mapped using a threshold of 3.5.

Table 7.

The selected mangrove forest sites in Southeast Asia, South America, Africa and Australia, and their respective geographical locations, dominant mangrove typology, and the lower minimum threshold utilized to map the mangroves.

| Region | Mangrove Site | Latitude | Longitude | Mangrove Type | MVI Threshold |
|----------------|--|---------------|----------------|------------------|---------------|
| Southeast Asia | Philippines (countrywide mean threshold) | 12°52'47" N | 121°46'26.5" E | Fringe | 3.5 |
| | Can Gio Mangrove Forest, Vietnam | 10°33'39.3" N | 106°52'08.6" E | Delta | 3.5 |
| | West Kalimantan, Indonesia | 0°39'59.0" S | 109°31'00.6" E | Delta | 3.5 |
| | Prey Nob, Cambodia | 10°40'43.9" N | 103°52'54.1" E | Fringe | 3 |
| South America | Mueang Trat District, Trat, Thailand | 12°08'59.1" N | 102°29'39.7" E | Fringe / Estuary | 3 |
| | Baia do Arraial, Amazon Coast, Brazil | 2°39'32.3" S | 44°09'49.2" W | Delta | 3 |
| Africa | Mabokweni, Tazania | 5°02'13.3" S | 39°04'27.1" E | Estuary | 3 |
| Australia | Prince Regent National Park, Western Australia | 15°16'49.9"S | 125°08'04.8"E | Estuary | 3 |

3.12 Index Uncertainties due to Tidal Level and Rainfall

The occurrence and magnitude of variations in mangrove area and mean MVI values due to differences in tidal and rainfall data were analyzed using multi-temporal data. MVI-derived mangrove area and mean mangrove MVI were examined against biophysical parameters, namely, FVC and C_w, and meteorological data, namely, precipitation (daily), 3-day aggregated precipitation, and tide level. Results show that satellite data acquired during the lowest tide among the dataset for Coron and Busuanga (-0.07 m) and Siargao (0.62 m) have generated the highest FVC and MVI-mapped mangrove areas (Table 8). FVC can provide quantitative information of the vegetation coverage status on the ground (Li et al, 2015). Higher FVC values during the lowest tide indicate detection of more mangrove vegetation canopy which will then affect the computation of MVI. Lower mangrove area estimates were obtained with increased tidal level from -0.07 m to 0.4 m for Coron and Busuanga. However, the magnitude of difference is low, ranging from minus 2.76 ha to 6.4 ha. This observation reflects the efficiency of MVI to map mangroves during low to mid-level tides even with the same lower MVI threshold. However, during higher tide events (0.68m), the area difference reaches to minus 23 ha for Busuanga and minus 43 ha for Coron as more mangroves are submerged and FVC is lower. This variation could be reduced by selecting a lower minimum MVI threshold for Sentinel-2 images acquired during higher tide. In example, using 7 as the minimum threshold for Siargao data collected on a lower tide and adjusting it to 6 for data collected on a higher tide yielded very close results (978 ha and 976 ha), as compared to using the same threshold for both data (Table 8, Siargao). Lowering the threshold allows inclusion of all mangroves within the tidal frame.

The tidal differences have also affected the NIR and SWIR reflectance, and the output MVI values. The data with the lowest tide resulted to the highest mean NIR values for all sites (Table 8). With increasing tide level, reduction in the NIR values was observed which is mainly due to the submersion of some mangroves and mangrove parts (Jia et al., 2019). As discussed earlier, reduction in NIR can lower the MVI formula dividend or the greenness information value, resulting to lower MVI. This can be observed in all sites where lower mean NIR yielded to lower mean mangrove MVI. The lowest mean NIR and mean MVI values were consistently recorded during high tide. The maximum difference between mangrove MVI values recorded during low to mid-level tides is only 0.5 for Busuanga and 0.2 for Coron. The Sentinel-2 images taken on January 2019 and January 2020, both acquired during lower tide levels, generated close MVI values of 8.1 and 8.2, respectively despite the one-year gap. The differences between per-site MVI values are higher during higher tides, with up to minus 1.2 for Busuanga, 1.3 for Coron, and 2.7 for Siargao.

High SWIR values were recorded during the highest tide and lowest tide, and lower during the mid-level tides. The difference among the SWIR1 values per site is lower than of NIR values, indicating that it has less effect on the MVI variation. SWIR1 value is known to be affected by soil background moisture (Herrmann et al., 2010) which is dependent on the soil properties. Mangrove substrate is known to be frequently waterlogged and is usually consist of clay loam with high water retention capacity. High SWIR reflectance of mangroves during the lowest tide could be connected with leaf water deficit (Kokaly et al., 2009), although some mangroves can store enough leaf moisture (Camilleri and Ribi, 1983; Nguyen et al, 2017).

Table 8.

Mean MVI metrics and the respective precipitation, tide, FVC, and C_w data for each satellite image acquired during the dry and wet seasons in Busuanga, Coron, and Siargao. Consistently, the highest mangrove area and highest mean mangrove MVI occurred for satellite data with the highest FVC value. These data with high FVC were all acquired during days with lower tide level. As tide level increases, the mangrove area and mean mangrove MVI decreases as more mangrove and non-mangrove parts are submerged in water. The effect of varying precipitation level during and before the data acquisition date yielded insignificant change in the canopy water content through C_w , and thus had minimal effect on mangrove reflectance and MVI values.

| Busuanga | Meteorological Data | | | Biophysical Data | | | MVI Metrics | | | | |
|------------------------|---------------------|--------------------------------|--------------------------------|------------------|----------|------------|--------------------|--------------------|----------|-----------|-------------------|
| | Season | Total Daily Precipitation (mm) | Total 3-day Precipitation (mm) | Tide level (m) | Mean FVC | Mean C_w | Min. MVI Threshold | Mangrove Area (ha) | Mean NIR | Mean SWIR | Mean Mangrove MVI |
| Jan 08, 2019 | Dry | 0 | 0.19 | 0.4 | 0.75 | 0.16 | 4.3 | 277.07 | 3421 | 751 | 8.1 |
| Jun 12, 2019 | Wet | 1.9 | 33.1 | 0.68 | 0.74 | 0.15 | 4.3 | 256.74 | 3192 | 819 | 7.4 |
| Dec 29, 2019 (Late) | Wet | 0 | 15.2 | -0.07 | 0.76 | 0.16 | 4.3 | 279.83 | 3489 | 763 | 8.6 |
| Jan 23, 2020 | Dry | 0 | 0 | 0.22 | 0.74 | 0.16 | 4.3 | 273.41 | 3332 | 735 | 8.2 |

| Coron | Meteorological Data | | | Biophysical Data | | | MVI Metrics | | | | |
|------------------------|---------------------|--------------------------------|--------------------------------|------------------|----------|------------|--------------------|--------------------|----------|-----------|-------------------|
| | Season | Total Daily Precipitation (mm) | Total 3-day Precipitation (mm) | Tide level (m) | Mean FVC | Mean C_w | Min. MVI Threshold | Mangrove Area (ha) | Mean NIR | Mean SWIR | Mean Mangrove MVI |
| Jan 08, 2019 | Dry | 0 | 0.15 | 0.4 | 0.70 | 0.14 | 4.3 | 253.8 | 3061 | 713 | 7.6 |
| Jun 12, 2019 | Wet | 5.9 | 36.8 | 0.68 | 0.67 | 0.12 | 4.3 | 215.56 | 2766 | 788 | 6.5 |
| Dec 29, 2019 (Late) | Wet | 0 | 23.31 | -0.07 | 0.73 | 0.14 | 4.3 | 258.76 | 3305 | 779 | 7.8 |
| Jan 23, 2020 | Dry | 0 | 0 | 0.22 | 0.71 | 0.14 | 4.3 | 254.92 | 3168 | 736 | 7.7 |

| Siargao | Meteorological Data | | | Biophysical Data | | | MVI Metrics | | | | |
|--------------|---------------------|--------------------------------|--------------------------------|------------------|----------|------------|--------------------|--------------------|----------|-----------|-------------------|
| | Season | Total Daily Precipitation (mm) | Total 3-day Precipitation (mm) | Tide level (m) | Mean FVC | Mean C_w | Min. MVI Threshold | Mangrove Area (ha) | Mean NIR | Mean SWIR | Mean Mangrove MVI |
| Feb 21, 2019 | Dry | 0 | 3.35 | 0.62 | 0.74 | 0.15 | 7 | 978 | 3286 | 743 | 12.8 |
| Aug 10, 2019 | Wet | 0 | 0.06 | 0.98 | 0.73 | 0.15 | 7 | 867 | 3127 | 739 | 10.1 |
| | | | | | | | 6 | 976 | 3117 | 752 | 9.7 |

Meanwhile, the effect of rainfall to the canopy water content is very minimal, with a difference of 0 to 1 in the C_w values despite varying amount of daily and 3-day aggregated precipitation. The data acquired December 29, 2019 and January 23, 2020 in Coron and Busuanga produced comparable MVI values and mangrove areas although up to 23 mm of rain occurred prior to acquisition of the earlier satellite images. The Coron-Busuanga and Siargao sites exhibit different tidal patterns during some months of the year due to their opposing locations, but the reducing effect of higher tides to the mean MVI values were similarly observed. This was taken in consideration in selecting the dates of satellite images used in the nationwide mapping.

4. Conclusion

This study provides an index built using green, NIR, and SWIR1 reflectance bands for discriminating mangrove from non-mangroves cover. Mangrove Vegetation Index, or MVI, measures the probability of a pixel to be a ‘mangrove’ by extracting the greenness and moisture information from the Sentinel-2 green, NIR and SWIR1 bands. The optimal MVI threshold from the study sites is from 4.5 to 20, but the lower threshold may be adjusted depending on the canopy density and coastal environment of the site. MVI have successfully discriminated visually and statistically the mangroves from non-mangroves cover types such as bare soil, built-up, terrestrial forest and terrestrial non-forest vegetation. The average index accuracy was 92%, validated through high resolution drone photos and field inventory data. Low to mid-level tidal height induced minimal variation on MVI values, while satellite data acquired during higher tides have less mean MVI due to reduced fractional cover of mangrove vegetation, affecting both the MVI greenness and moisture equations. Lowering the MVI threshold is necessary unless only satellite data collected during lower tidal events will be selected.

Stressed mangrove trees gave lower MVI values, while totally damaged and dead trees generated an MVI value outside the mangrove threshold. However, comparison with vegetation health indicators such as NDVI, FVC and LAI in riverine and fringe mangrove forests suggested that the MVI value does not always increase with increasing vegetation health, but rather increase with higher probability of a pixel being classified as ‘mangroves’ based on the greenness and moisture information. This was further validated by correlating the MVI values with Sentinel-2 SNAP-derived chlorophyll-a (C_a) and canopy water content (C_w). MVI was strongly and positively correlated with C_w and C_a which suggest that the MVI can efficiently measure greenness and moisture in the canopy level. The MVI formula was applied to Landsat-8 data using the equivalent green, NIR and SWIR1 data. The Landsat and Sentinel-2 bands had moderate agreement in the green and NIR regions, and high in the SWIR1 region. The Landsat MVI had wider threshold range and has higher values than Sentinel-2 in most of the sample plots, but the optimal minimum threshold is the same which is 4.5 and/or 4.6 for the case of the Philippines. Similar mangrove area locations were detected between the two sensors.

This study developed two mangrove mapping automation tools, the IDL-based and Google Earth Engine-based MVI Mapper. The IDL MVI Mapper can be used offline when the input data is already downloaded, while the Google Earth Engine GUI can be operated online without the need to locally download the input Sentinel-2 bands. Further, the study mapped the mangrove extent in the Philippines using the GEE workflow to generate an updated mangrove map with higher resolution (10m). The MVI was also applied to four other countries in Southeast Asia: Thailand, Vietnam, Indonesia and Cambodia. Although lower minimum thresholds were selected compared with Philippine sites, the MVI can still separate the mangrove from non-mangrove cover with the said adjusted thresholds, generating mangrove area estimates close to previous estimates obtained from previous studies in the said sites. Further application of MVI to mangrove forests in Brazil, Tazania, and Western Australia showed similar thresholds with the mangrove sites in Southeast Asia. Other MVI applications such as mangrove spatiotemporal analysis, change detection and automatic site-specific threshold detection can be further explored in future works. MVI can be used for rapid and accurate mangrove mapping because of the non-complex input data, simple index calculation, high initial index accuracy, universality of the index which is applicable to other satellite data, and the availability of automation tools.

Author contributions

Alvin Baloloy and Ariel Blanco conceptualized the ideas and design of the study including data collection and analysis; Raymund Sta. Ana contributed in the automation of the mapping workflow; and Kazuo Nadaoka assisted in assessing and reviewing the applicability of the index. All authors contributed in writing the manuscript.

Declaration of competing interest

The authors declare that they have no known competing financial interests or personal relationships that could have appeared to influence the work reported in this paper.

Acknowledgements

This research work was done under the ‘The Project for Comprehensive Assessment and Conservation of Blue Carbon Ecosystems and their Services in the Coral Triangle (BlueCARES) funded by Japan International Cooperation Agency (JICA) and Japan Science and Technology Agency (JST) under the SATREPS Program. Most of the validation data were acquired during the ‘Integrated Assessment and Modelling of Blue Carbon Ecosystems for Conservation and Adaptive Management’ (IAMBlueCECAM) Project 1: Mangrove Remote Sensing using LiDAR, RADAR, Multispectral and Hyperspectral Data (MaRS, Project No. 04038) funded by the DOST Philippine Council for Industry, Energy and Emerging Technology Research and Development (PCIEERD). Utmost acknowledgement is given to the Nationwide Detailed Resource Assessment Using LiDAR (Phil-LiDAR 2) for the Masinloc field inventory data. Further, the researchers would like to thank the Environmental Systems Applications of Geomatics Engineering (EnviSAGE) laboratory for the equipment and assistance given in conducting the study.

References

- Alongi, D.M., 2002. Present state and future of the world’s mangrove forests. Environ. Conserv. 29, 331-349. <https://doi.org/10.1017/S0376892902000231>
- Al-Saidi, A., Fukuzawa, Y., Ueno, M., Baba, S., Kawamitsu, Y. 2009. Temporal and vertical variations in photosynthetic drivers in mangrove canopies, Okinawa, Japan. Plant Prod. Sci. 12, 336- 340. <https://doi.org/10.1626/pps.12.336>
- Alsaideh, B., Al-Hanbali, A., Tateishi, R., Kobayashi, T., Thanh Hoan, N. 2013. Mangrove Forests Mapping in the Southern Part of Japan Using Landsat ETM+ with DEM. J. Geogr. Inf. Syst. 5, 369-377. <http://dx.doi.org/10.4236/jgis.2013.54035>
- Araujo, R.J., Jaramillo, J.C., Snedaker, S.C. 1997. LAI and leaf size differences in two red mangrove forest types in South Florida. Bulletin of Marine Science, 60(3): 643-647.
- Ashraf, M.A., Maah, M.J., Yusoff, I. 2011. Introduction to Remote Sensing of biomass, biomass and Remote Sensing of biomass. Dr. Islam Atazadeh (Ed.), ISBN: 978-953-307-490-0. InTech. <https://doi.org/10.5772/16462>
- Basheer, M.A., Kafrawy, S.B., Mekawy, A. 2019. Identification of mangrove plant using hyperspectral remote sensing data along the Red Sea, Egypt. Egyptian Journal of Aquatic Biology & Fisheries. 23, 27-36. <https://doi.org/10.21608/ejabf.2019.25932>
- Bowman, K.P. 2004. An introduction to computer programming using Interactive Data Language (IDL). Department of Atmospheric Sciences Texas A&M University. <http://read.pudn.com/downloads91/ebook/352317/LearningIDL.pdf>
- Bunting P., Rosenqvist, A., Lucas R., Rebelo L-M., Hilarides L., Thomas, N., Hardy, A., Itoh, T., Shimada M., Finlayson, C.M. 2018. The Global Mangrove Watch – a new 2010 global baseline of mangrove extent. Remote Sens. 10, 1669. <https://doi.org/10.3390/rs10101669>
- Cahoon, D. R., Hensel, P., Rybczyk, J., McKee, K. L., Proffitt, C. E., Perez, B. C. 2003. Mass tree mortality leads to mangrove peat collapse at Bay Islands, Honduras after Hurricane Mitch. Journal of Ecology. 91, 1093–1105. <http://doi.org/10.1046/j.1365-2745.2003.00841.x>
- Camilleri, J.C., Ribi, G. 1983. Leaf thickness of mangroves (*Rhizophora mangle*) growing in different salinities. Biotropica. 15, 139-141. <http://doi.org/10.2307/2387959>

- Cierniewski, J., Kuśnierzek, K. 2010. Influence of several soil properties on soil surface reflectance. *Quaestiones Geographicae*. 29, 13-25. <https://doi.org/10.2478/v10117-010-0002-9>
- Claverie, M., Ju, J., Masek, J.G., Dungan, J.L., Vermote, E.F., Roger, J.C., Skakun, S.V., Justice, C. 2018. The harmonized Landsat and Sentinel-2 surface reflectance dataset. *Remote Sens. Environ.* 219, 145–161. <https://doi.org/10.1016/j.rse.2018.09.002>
- Clough, B.F. 1993. Conservation and sustainable utilization of mangrove forests and their present state of conservation in the South-east Asia/Pacific Region. *Mangrove Ecosystems Technical Reports No. 1*, Okinawa, Japan. International Society for Mangrove Ecosystems, 202.
- Cresswell, I.D., Semeniuk, V. 2011. Mangroves of the Kimberley Coast: ecological patterns in a tropical ria coast setting. *J R Soc. West Aust.* 94, 213-237. <http://hdl.handle.net/102.100.100/104152?index=1>
- Crooks, S., Herr, D., Tamelander, J., Laffoley, D., Vandever, J. 2011. Mitigating climate change through restoration and management of coastal wetlands and near-shore marine ecosystems: challenges and opportunities. Environment Department, Paper 121, World Bank, Washington, DC. <http://hdl.handle.net/10986/18318>
- Cunha-Lignon, M., Coelho Jr., C., Almeida, R., Menghini, R.P., Schaeffer-Novelli, Y., Cintrón, G., Dahdouh-Guebas, F. 2011. Characterisation of mangrove forest types in view of conservation and management: a review of mangals at the Cananéia region, São Paulo State, Brazil. *J. Coast. Res.* 64, 349-353. ISSN 0749-0208.
- Dangan-Galon, F., Dolorosa, R.G., Sespeñe, J.S., Mendoza, N. 2016. Diversity and structural complexity of mangrove forest along Puerto Princesa Bay, Palawan Island, Philippines. *Journal of Marine and Island Cultures*. 5, 118-125. <https://doi.org/10.1016/j.jmic.2016.09.001>
- Deilmai, B.R., Ahmad, B.B., Zabihi, H. 2012. Comparison of two classification methods (MLC and SVM) to extract land use and land cover in Johor Malaysia. *IOP Conf Ser Earth Environ Sci.* 20, 1-6. <http://dx.doi.org/10.1088/1755-1315/20/1/012052>
- Diop, E.S. (1993) Conservation and sustainable utilization of mangrove forests and their present state of conservation in Latin America and Africa regions. Technical Reports, Volume 3. Okinawa, Japan. International Society for Mangrove Ecosystems. 262.
- Ellison, J.C. 2000. How South Pacific mangroves may respond to predicted climate change and sea level rise. Chapter 15, pages 289-301, In: Gillespie, A., and Burns, W. (eds), *Climate change in the South Pacific: impacts and responses in Australia, New Zealand, and small island states*. Kluwer Academic Publishers, Dordrecht, Netherlands. https://doi.org/10.1007/0-306-47981-8_16
- European Space Agency. The Copernicus Open Access Hub. Available online: <https://scihub.copernicus.eu> (accessed on August 2018).
- Ewel, K.C., Twilley, R.R., Ong, J.E. 1998. Different kinds of mangrove forests provide different goods and services. *Global Ecol Biogeogr.* 7, 83-9. <https://doi.org/10.1111/j.1466-8238.1998.00275.x>
- Food Agric. Organ. U. N. (FAO). 2003. Status and trends in mangrove area extent worldwide. *Work. Pap. FRA 63*, FAO, Rome, Italy. 14.
- Food Agric. Organ. U. N. (FAO), UNEP. 1981. Tropical Forest Resources Assessment Project, Forest Resources of Tropical Asia. Green RO, Pavri BE and Chrien TG (2003) On orbit radiometric and spectral calibration characteristics of EO-1 Hyperion derived with an underflight of AVIRIS and in situ measurements at Salar de Arizaro, Argentina. *Rem Sens Envir.* 41, 1194–1203. <http://doi.org/10.1109/TGRS.2003.813204>
- Farnsworth, E.J.; Ellison, A.M., 1998. The global conservation status of mangroves. *Oceanogr. Lit. Rev.* 1,138–139. <http://reforestation.elti.org/resource/212/>
- Field, C.D. 1995. Impact of expected climate change on mangroves. *Hydrobiologia*. 295, 75. <https://doi.org/10.1007/BF00029113>
- Fourty, T., Baret, F. 1997. Amélioration de la précision des coefficients d'absorption spécifiques de la matière sèche et des pigments photosynthétiques. INRA Bioclimatologie. 35.
- Garces, L.R., Pido, M.D., Tupper, M.H., Silvestre, G.T. 2012. Evaluating the management effectiveness of three marine protected areas in the Calamianes Island, Palawan Province, Philippines: Process, selected results and their implications for planning and management. *Ocean. Coast. Manage.* 1-9. <http://dx.doi.org/10.1016/j.ocecoaman.2012.07.014>
- Ghandi, S., Jones, T.G. 2019. Identifying mangrove deforestation hotspots in South Asia, Southeast Asia and Asia-Pacific. *Remote Sens.* 11, 728. <https://doi.org/10.3390/rs11060728>
- Giri, C., Muhlhausen, J., 2008. Mangrove forest distribution and dynamics in Madagascar (1975–2005). *Sensors* 8, 2104–2117. <https://doi.org/10.3390/s8042104>
- Górská, A., Lazor, J.W., Zwieniecka, A.K., Benway, C., Zwieniecki, M. A. 2010. The capacity for nitrate regulation of root hydraulic properties correlates with species' nitrate uptake rates. *Plant Soil.* 337, 447–455. <https://doi.org/10.1007/s11104-010-0540-x>
- Green, R. O., Pavri, B.E., Chrien, T.G. 2003. On-Orbit radiometric and spectral calibration characteristics of EO-1 Hyperion derived with an underflight of AVIRIS and in situ measurements at Salar de Arizaro, Argentina. *IEEE T Geosci Remote.* 41, 1194-1203. <http://doi.org/10.1109/TGRS.2003.813204>
- Gupta, K., Mukhopadhyah, A., Giri, S., Chanda, A., Majumdar, S.D., Samanta, S., Mitra, D., Samal, R.N., Pattnaik, A.K., Hazra, S. 2018. An Index for discrimination of mangroves from non-mangroves using Landsat 8 OLI imagery. *MethodsX*. 5, 1129-1139. <https://doi.org/10.1016/j.mex.2018.09.011>

- HCMC, 2017. Decision No. 3901 on approving the areas of forest and land in HCM city in 2016. Ho Chi Minh: The people's committee of HCM city.
- Herrmann, I., Karnieli, A., Bonfil, D.J., Cohen, Y., Alchanatis, V. 2010. V. SWIR-based spectral indices for assessing nitrogen content in potato fields. *Int. J. Remote Sens.* 31, 5127–5143. <https://doi.org/10.1080/01431160903283892>
- Hoa, N.H., Binh, T.D. 2016. Using Landsat imagery and vegetation indices differencing to detect mangroves change: a case study in Thai Thuy District, Thai Province. *J. of For. Sci. & Tech.* 5, 59-66.
- Hopper, M. 2007. WXTide32 software. <http://WXTide32.com>
- Huete, A.R. 2004. Remote Sensing for Environmental Monitoring in: *Environmental Monitoring and Characterization*. <https://doi.org/10.1016/B978-012064477-3/50013-8>
- Huete, A.R., 1988. A soil adjusted vegetation index (SAVI). *Remote Sens. Environ.* 25, 295-309. [https://doi.org/10.1016/0034-4257\(88\)90106-X](https://doi.org/10.1016/0034-4257(88)90106-X)
- Hung, T.T., Huyen, D.T., Tu, T.A., Desmet, M. 2018. Presence of trace elements in sediment of Can Gio mangrove forest, Ho Chi Minh City, Vietnam. *Vietnam Journal of Earth Sciences.* 41, 25-31. <https://doi.org/10.15625/0866-7187/41/1/13543>
- Jacquemoud, S., Baret, F., 1990. Prospect - a model of leaf optical-properties spectra. *Remote Sens. Environ.* 34, 75-91. [https://doi.org/10.1016/0034-4257\(90\)90100-Z](https://doi.org/10.1016/0034-4257(90)90100-Z)
- Ji, L., Zhang, L., Wylie, B. 2009. Analysis of dynamic thresholds for the normalized difference water index. *Photogramm. Eng. Remote Sens.* 75, 1307–1317. <https://doi.org/10.14358/PERS.75.11.1307>
- Jia, M., Wang, Z., Wang, C., Mao, D., Zhang, Y. 2019. A new vegetation index to detect periodically submerged Mangrove forest using Single-Tide Sentinel-2 Imagery. *Remote Sens.* 11, 2043; <https://doi.org/10.3390/rs11172043>
- Jordan, C.F., 1969. Derivation of leaf-area index from quality of light on the forest floor. *Ecology.* 50, 663–666. <http://doi.org/10.2307/1936256>
- Jusoff, K. 2006. Individual mangrove species identification and mapping in Port Klang using airborne hyperspectral imaging. *J Sustainable Sci Manage.* 1, 27-36.
- Kamal, M., Phinn, S., Johansen, K. 2015. Object-based approach for multi-scale mangrove composition mapping using multi-resolution image datasets. *Remote Sens.* 7, 4753-4783. <https://doi.org/10.3390/rs70404753>
- Kamal, M., Phinn, S. 2011. Hyperspectral data for mangrove species mapping: a comparison of pixel-based and object based approach. *Remote Sens.* 3, 2222-2242. <https://doi.org/10.3390/rs3102222>
- Kamaruzaman, J., Kasawani, I. 2007. Imaging Spectrometry on Mangrove Species Identification and Mapping in Malaysia. *WSEAS Transactions on Biology and Biomedicine.* 4, 118-126. <http://psasir.upm.edu.my/id/eprint/7723>
- Kanniah, K.D., Sheikhi, A., Cracknell, A.P., Goh, H.C., Tan, K.P., Ho, C.S., Rasli, F.N. 2015. Satellite images for monitoring mangrove cover changes in a fast growing economic region in Southern Peninsular Malaysia. *Remote Sens.* 7, 14360-14385. <http://doi.org/10.3390/rs71114360>
- Kathiresan, K., Bingham, B.L. 2001. Biology of mangroves and mangrove ecosystems. *Advances in Marine Biology.* 40, 81-251. [https://doi.org/10.1016/S0065-2881\(01\)40003-4](https://doi.org/10.1016/S0065-2881(01)40003-4)
- Kokaly, R.F., Asner G.P., Ollinger S.V., Martin M.E., Wessman C.A. 2009. Characterizing canopy biochemistry from imaging spectroscopy and its application to ecosystem studies. *Remote Sens. Environ.* 113, 78-91. <http://doi.org/10.1016/j.rse.2008.10.018>
- Kongwongjan, J., Suwanprasit, C., Thongchumnum, P. 2012. Comparison of vegetation indices for mangrove mapping using THEOS data. *Proceedings of the Asia-Pacific Advanced Network.* 33, 56-64. <http://dx.doi.org/10.7125/APAN.33.6>
- Kovacs, J.M., Wang, J., Blanco-Correa, M. 2001. Mapping disturbances in a mangrove forest using multi-date Landsat TM imagery. *Environ. Manag.* 27, 763-776. <https://doi.org/10.1007/s002670010186>
- Kumar, T., Mandal, A., Dutta, D., Nagaraja, R., Dadhwali, V.K. 2019. *Geocarto Int.* 34, 415-442. <https://doi.org/10.1080/10106049.2017.1408699>
- Lawas, L.M. 1974. Economic study on alternative uses of mangrove swamps: bakawan production or fish ponds. In: *Proceedings of Indo-Pacific Fishery Council*, 65-69. 15th Session. 18-27 October 1972, Wellington, New Zealand, Section 2 Bangkok, FAO.
- Li, S., Ganguly, S., Dungan, J.L., Wang, W. 2017. Nemaní, R.R. Sentinel-2 MSI radiometric characterization and cross-calibration with Landsat-8 OLI. *Adv. Remote Sens.* 6, 147. <https://doi.org/10.4236/ars.2017.62011>
- Li, Y., Wang, H., Li, X.B. 2015. Fractional vegetation cover estimation based on an improved selective endmember spectral mixture model. *PLoS ONE* 10. 4. <https://doi.org/10.1371/journal.pone.0124608>
- Lin, P., Fu, Qin. 1995. Environment, ecology and economic utilization of mangrove in China. Higher Education Press, Beijing, China.
- Liu, K., Li, X., Shi, X., Wang, S. 2008. Monitoring mangrove changes using remote sensing and GIS data with decision-tree learning. *Wetlands.* 28, 336–346. <https://doi.org/10.1672/06-91.1>

- Long, J.B., Giri, C. 2011. Mapping the Philippines' mangrove forests using Landsat imagery. Sensors. 11, 2972-2981. <http://doi.org/10.3390/s110302972>
- Lovelock, C.E., Ball, M.C., Martin, K.C., Ferrer, I.C. 2009. Nutrient enrichment increases mortality of mangroves. PLoS ONE. 4, e5600. <https://doi.org/10.1371/journal.pone.0005600>
- Lu D., Weng Q.A. 2007. A survey of image classification methods and techniques for improving classification performance. Int. J. Remote Sens. 28, 823-870. <http://doi.org/10.1080/01431160600746456>
- Lucas, R., Mitchell, A., Bunting, P. 2008. Hyperspectral data for assessing carbon dynamics and biodiversity of forests. In: Hyperspectral Remote Sensing of tropical and sub-tropical forests, Kalacska, M. & Sanchez-Azofeifa, G.A. (1) 50-51. ISBN 9781420053418.
- Ma, L., Li, M., Ma, X., Cheng, L., Du, P., Liu, Y. 2017. A review of supervised object-based land-cover image classification. ISPRS J. Photogramm. Remote Sens. 130, 277-293. <https://doi.org/10.1016/j.isprsjprs.2017.06.001>
- Main-Knorn, M., Pflug, B., Debaecker, V., Louis, J. 2015. Calibration and validation plan for the L2A processor and products of the Sentinel-2 Mission. ISPRS Ann. Photogramm. Remote Sens. Spat. Inf. Sci. 40, 1249-1255. <http://doi.org/10.5194/isprsarchives-XL-7-W3-1249-2015>
- Manna, S., Raychaudhuri, B. 2018. Mapping distribution of Sundarban mangroves using Sentinel-2 data and new spectral metric for detecting their health condition. Geocarto International. 1-20. <https://doi.org/10.1080/10106049.2018.1520923>
- Newnam, G.J., Burt, T. 2001. Validation of leaf reflectance and transmittance model for three agricultural crop species. IEEE Trans Geosci Remote Sens. 2976-2978. <http://doi.org/10.1109/IGARSS.2001.978227>
- Nguyen, H.T., Meir, P., Sack, L., Evans, J.R., Oliveira, R.S., Ball, M. 2017. Leaf water storage increases with salinity and aridity in the mangrove *Avicennia marina*: integration of leaf structure, osmotic adjustment and access to multiple water sources Plant Cell Environ. 40, 1576-9. <https://doi.org/10.1111/pce.12962>
- Nugroho, T.S., Fahrudin, A., Yulianda, F., Bengen, D. 2019. Structure and composition of riverine and fringe mangroves at Muara Kubu protected areas. AACL Bioflux, 12, 378-393. <http://www.bioflux.com.ro/docs/2019.378-393.pdf>
- Patterson, W.G., 1986. Mangrove Community Boundary Interpretation and Detection of Areal Changes in Marco Island, Florida: Application of Digital Image Processing and Remote Sensing Techniques, U.S. Fish and Wildlife Service Biological Report. 86, 1-87.
- Pekel, J.F., Cottam, A., Gorelick, N., Belward, A.S. 2016. High-resolution mapping of global surface water and its long-term changes. Nature. 540, 418-422. <https://doi.org/10.1038/nature20584>
- Pham, L.T.H., Vo, T.Q., Dang, T.D., Nguyen, U.T.N. 2019. Monitoring mangrove association changes in the Can Gio biosphere reserve and implications for management. Remote Sensing Applications: Society and Environment, 13, 298-305. <https://doi.org/10.1016/j.rsase.2018.11.009>
- Philippine Council for Agriculture, Forestry and Natural Resources Research and Development. 1991. The Philippines recommends for mangrove production and harvesting. Philippines Recommends series No.74. PCARRD / DENR. 96. ISBN 971-20-0188-1.
- Pimple, U., Simonetti, D., Sitthi, A., Pungkul, S., Leadprathom, K., Skupek, H., Som-ard, J., Gond, V., Towprayoon, S. 2018. Google earth engine based three decadal landsat imagery analysis for mapping of mangrove forests and its surroundings in the Trat province of Thailand. Journal of Computer and Communications.6, 247-264. <http://doi.org/10.4236/jcc.2018.61025>
- Prasad, K.A., Gnanappazham. 2015. Multiple statistical approaches for the discrimination of mangrove species of *Rhizophoraceae* using transformed field and laboratory hyperspectral data. Geocarto Int. 31, 891-912. <https://doi.org/10.1080/10106049.2015.1094521>
- Primavera, J.H. 2000. Development and conservation of Philippine mangroves: Institutional issues. Ecol. Econ. 35, 91-106. [https://doi.org/10.1016/S0921-8009\(00\)00170-1](https://doi.org/10.1016/S0921-8009(00)00170-1)
- Primavera, J.H. 2005. Mangroves, Fishponds, and the Quest for Sustainability. Science. 310, 57-59. <http://doi.org/10.1126/science.1115179>
- Pumijumnong, N. 2014. Mangrove Forests in Thailand. In: Faridah-Hanum I., Latiff A., Hakeem K., Ozturk M. (eds) Mangrove Ecosystems of Asia. Springer, New York, NY. https://doi.org/10.1007/978-1-4614-8582-7_4
- Rasel, S. M. M., Chang, H.C., Diti, I.J., Ralph, T., Saintilan, N. 2016. Comparative analysis of Worldview-2 and Landsat 8 for coastal saltmarsh mapping accuracy assessment. Proc. SPIE 9864, Sensing for Agriculture and Food Quality and Safety VIII, 986409. <https://doi.org/10.1117/12.2222960>
- Raven, P.H., Evert, R.F., Eichhorn, S.E. 1992. Biology of plants. W. H. Freeman & Company Press, New York, NY.
- Razali, S.M., Nuruddin, A.A., Lion, M. 2019. Mangrove vegetation health assessment based on remote sensing indices for Tanjung Piai, Malay Peninsular. J. Landsc. Ecol. 12, 26-40. <https://doi.org/10.2478/jlecol-2019-0008>
- Reef, R., Lovelock, C.E. 2014. Regulation of water balance in mangroves. Ann Bot. 115, 385-95. <http://doi.org/10.1093/aob/mcu174>
- Romañach, S.S., DeAngelis, D.L., Koh, H.L., Li, Y., Teh, S.Y., Raja Barizan, R.S., Zhai, L. 2018. Conservation and restoration of mangroves: Global status, perspectives, and prognosis. Ocean Coast. Manag. 154, 72-82. <https://doi.org/10.1016/j.ocecoaman.2018.01.009>

- Roslani, M.A., Mustapha, M.A., Lihan, T., Wan Juliana, W.A. 2003. Classification of mangroves vegetation species using texture analysis on RapidEye satellite imagery. AIP Conference Proceedings. 1571, 480. <https://doi.org/10.1063/1.4858701>
- Rouse, J.W., Has, R.H., Schell, J.A., Deering, D.W. 1973. Monitoring vegetation systems in the Great Plains with ERTS. In Proceedings of the Third ERTS Symposium (NASA), Washington, DC, USA, SP-351 I, 309-317.
- Rullan-Silva, C.D., Olthoff, A.E., Delgado de la Mata, J.A., Pajares-Alonso, J.A. 2013. Remote Monitoring of Forest Insect Defoliation - A Review. For. Syst. 22, 377. <http://doi.org/10.5424/fs/2013223-04417>
- Runge, A., Grosse, G. 2019. Comparing spectral characteristics of Landsat-8 and Sentinel-2 same-day data for arctic-boreal regions. Remote Sens., 11, 1-29. <https://doi.org/10.3390/rs11141730>
- Sandalo, R.M., Baltazar, T. 1997. The Palawan Biosphere Reserve: Philippines. Working Papers No. 19, 1997. Paris, France: UNESCO. South-South Cooperation Programme for Environmentally Sound Socio-Economic Development in the Humid Tropics.
- Schmidt, G., Jenkerson, C., Masek, J., Vermote, E., Gao, F. 2013. Landsat ecosystem disturbance adaptive processing system (LEDAPS) algorithm description. In: US Geological Survey. <https://doi.org/10.3133/ofr20131057>
- Sharma, S., Yasuoka, J., Nakamura, T., Watanabe, A., Nadaoka, K. 2014. The Role of hydroperiod, soil moisture and distance from the river mouth on soil organic matter in Fukido Mangrove Forest, Ishigaki Island, Japan. In Proceeding of the Intl. Conf. on Advances In Applied Science and Environmental Engineering. 2014. ISBN: 978-1-63248-004-0.
- Sikdar, D., Banerjee, A., Das, P., Datta, S. 2016. Biodegradation of Acenaphthene Using Two Different Isolated Bacteria: Comparative Analysis and Optimization Using Artificial Neural Network. Environmental Pollution and Protection. 1, 12-22. <http://dx.doi.org/10.22606/epp.2016.11002>
- Souza-Filho, P.W. 2005. Costa de manguezais de macromaré da Amazônia: cenários morfológicos, mapeamento e quantificação de áreas usando dados de sensores remotos. Revista Brasileira de Geofísica. 23, 427-435. <https://doi.org/10.1590/S0102-261X2005000400006>
- Spalding, M., Blasco, F., Field C.,eds. 1997. World Mangrove Atlas. Okinawa, JP. Int. Soc. Mangrove Ecosyst. 178.
- Spalding, M., Kainuma, M., Collins, L. 2010. World Atlas of Mangroves. Earthscan, London, Washington DC, 319.
- Tieng, T., Sharma, S., MacKenzie, R.A., Venkattappa, M., Sasaki, N.K., Collin, A. 2019. Mapping mangrove forest cover using Landsat-8 imagery, Sentinel-2, very high resolution images and Google Earth Engine algorithm for entire Cambodia. IOP Conf. Series: Earth and Environmental Science. 266. <http://doi.org/doi:10.1088/1755-1315/266/1/012010>
- Tomlinson, P.B. 1994. The botany of mangroves. Cambridge, UK: Cambridge University Press. <https://doi.org/10.1017/CBO9781139946575>
- Tucker, C.J. 1980. Remote sensing of leaf water content in the near infrared. Remote Sens Environ. 10:13–32.
- Tyerman, S. D., Wignes, J. A., Kaiser, B. N. 2017. “Root Hydraulic and Aquaporin Responses to N Availability,” in Plant Aquaporins, eds F. Chaumont and S. Tyerman (Cham: Springer). 207–236.
- Veetttil, B.K., Pereira, S.R.F., Quang, N.X., 2018. Rapidly diminishing mangrove forests in Myanmar (Burma): A Review. Hydrobiologia. 822, 19-35. <http://doi.org/10.1007/s10750-018-3673-1>
- Villamayor, B.M.R., Rollon, R.N., Samson, M.S., Albano, G.M.G., Primavera J. H. 2016. Impact of Haiyan on Philippine mangroves: Implications to the fate of the widespread monospecific Rhizophora plantations against strong typhoons. Ocean Coast Manage. 132, 1–14. <https://doi.org/10.1016/j.ocecoaman.2016.07.011>
- Wang, D., Wan, B., Qiu, P., Zuo, Z., Wang, R., Wu, X. 2018. Evaluating the Performance of Sentinel-2, Landsat 8 and Pléiades-1 in Mapping Mangrove Extent and Species. Remote Sens. 10, 1468. <https://doi.org/10.3390/rs10091468>
- Weiss M., Baret F. 2016. S2ToolBox Level 2 products: LAI, FAPAR, FCover. Accessed on 12 September 2018. Available online: http://step.esa.int/docs/extr/ATBD_S2ToolBox_L2B_V1.1.pdf
- Winarsa, G., Purwanto, A.D., Yuwono, D.M. 2014. New mangrove index as degradation / health indicator using Remote Sensing data: Segara Anakan and Alas Purwo case study. 12th Biennial Conference of Pan Ocean Remote Sensing Conference.
- Zhang, C., Kovacs, J.M., Liu, Y., Flores-Verdugo,F., Flores-de-Santiag, F. 2014. Separating Mangrove Species and Conditions Using Laboratory Hyperspectral Data: A Case Study of a Degraded Mangrove Forest of the Mexican Pacific. Remote Sens. 6, 11673-11688. <https://doi.org/10.3390/rs61211673>
- Zhang, X., Tian, Q. 2013. A mangrove recognition index for remote sensing of mangrove forest from space. Current Science. 105, 1149-1154.
- Zhang, X., Treitz, P.M., Chen, D., Quan, C., Shi,L., Li, X. 2017. Mapping mangrove forests using multi-tidal remotely-sensed data and a decision-tree-based procedure. Int J Appl Earth Obs Geoinformation. 62, 201-214. <https://doi.org/10.1016/j.jag.2017.06.010>